Article

Fluorination Enables Dual Ferroelectricity in Both Solid- and Liquid-Crystal Phases

Jun-Chao Liu,[†] Hang Peng,[†] Xiao-Gang Chen, Hui-Peng Lv, Xian-Jiang Song, Ren-Gen Xiong, and Wei-Qiang Liao*

Cite This: *JACS Au* 2023, 3, 1196−1204

Read Online

ACCESS | 📊 Metrics & More | 📖 Article Recommendations | 🔲 Supporting Information

ABSTRACT: Ferroelectric materials are a special type of polar substances, including solids or liquid crystals. However, obtaining a material to be ferroelectric in both its solid crystal (SC) and liquid crystal (LC) phases is a great challenge. Moreover, although cholesteric LCs inherently possess the advantage of high fluidity, their ferroelectricity remains unknown. Here, through the reasonable H/F substitution on the fourth position of the phenyl group of the parent nonferroelectric dihydrocholesteryl benzoate, we designed ferroelectric dihydrocholesteryl 4-fluorobenzoate (4-F-BDC), which shows ferroelectricity in both SC and cholesteric LC phases. The fluorination induces a lower symmetric polar $P1$ space group and a new solid-to-solid phase transition in 4-F-BDC. Beneficial from fluorination, the SC and cholesteric LC phases of 4-F-BDC show clear ferroelectricity, as confirmed by well-shaped polarization−voltage hysteresis loops. The dual ferroelectricity in both SC and cholesteric LC phases of a single material was rarely found. This work offers a viable case for the exploration of the interplay between ferroelectric SC and LC phases and provides an efficient approach for designing ferroelectrics with dual ferroelectricity and cholesteric ferroelectric liquid crystals.

KEYWORDS: *ferroelectricity, molecular ferroelectrics, phase transition, solid crystal, liquid crystal*
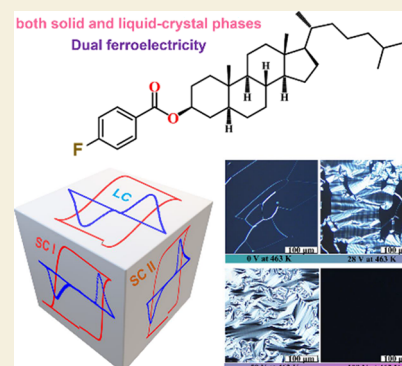
INTRODUCTION

Ferroelectricity describes switchable spontaneous electrical polarization that can exist in polar substances of either solid or liquid crystals.[1−3] The history of ferroelectrics began with the disclosure of a peculiar dielectric behavior of solid crystal (SC) Rochelle salt in 1920,[4] and in the following century, various types of ferroelectric solids emerged, including inorganic crystals or ceramics,[5,6] molecular crystals,[7−12] and polymers.[13,14] Their switchable polarization features with excellent electrical, mechanical, and optical properties have been extensively studied and widely used in memory elements, capacitors, transducers, actuators, and sensors.[15,16] The connection between ferroelectricity and liquid crystals (LCs) started in 1975 with the discovery of the first ferroelectric LC DOBAMBC.[17] Ferroelectric LCs have unique application advantages in display and optoelectronics due to their exceptionally fast electro-optical response and the special photoelectric effect.[18−22] For a long time, compared to other types of LC phases with $D_{\infty h}$ symmetry, the chiral smectic LC phase was thought to exhibit ferroelectricity because of the C_2-symmetric polarization vector perpendicular to both the director and the molecular layer direction.[23−33] Subversively, in recent years, ferroelectricity has also been experimentally proved in the nematic LCs with $C_{\infty v}$ symmetry, breaking the conventional thinking of ferroelectric LCs and opening a new chapter in condensed matter science and related applica-

tions.[34−39] The broken head-to-tail symmetry of two permissible director orientations in such a nematic LC system enables the molecular dipoles to spontaneously orient to a preferred direction, generating macroscopic polarization.[34,40−42] Liquid crystals can be generated by heating some organic solid crystals.[43] However, although the respective development of ferroelectric SCs and LCs has made great strides, and most recently a molecular ferroelectric with ferroelectricity in the SC and typical chiral smectic LC phases has been reported,[44] it still remains a great challenge to design a single material with ferroelectricity in both its SC and LC phases. The dual ferroelectricity in one material is fascinating and provides a platform for in-depth studying and understanding of the underlying correlation of the symmetry and polarity between sequential SC and LC phases. Moreover, it serves as an alternative in future electro-optical applications such as optical switches, modulators, and attenuators working in a relatively wide temperature range.[19]
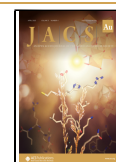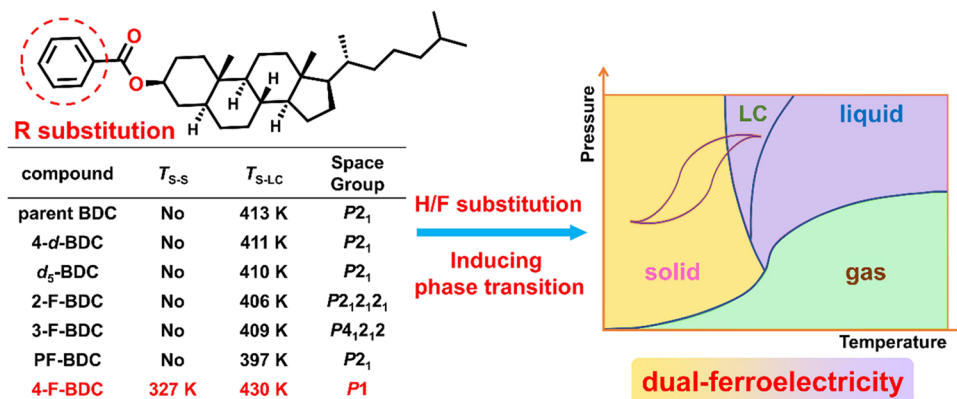
Scheme 1. Chemical Design Strategy of H/F Substitution for the Dual Ferroelectricity in Both SC and LC Phases of 4-F-BDC[a]

compound	T_{S-S}	T_{S-LC}	Space Group
parent BDC	No	413 K	$P2_1$
4-d-BDC	No	411 K	$P2_1$
d_5-BDC	No	410 K	$P2_1$
2-F-BDC	No	406 K	$P2_12_12_1$
3-F-BDC	No	409 K	$P4_12_12$
PF-BDC	No	397 K	$P2_1$
4-F-BDC	327 K	430 K	$P1$

[a]The T_{S-S} and T_{S-LC} denote the phase transition temperature of solid-to-solid and solid-to-liquid crystal phase transition, respectively.

To produce ferroelectricity with nonzero macroscopic polarization, the mirror symmetry perpendicular to the polarization director should be broken. The local symmetry of the LC phase must be such that the polarization in at least one direction is not canceled by any symmetry operation, while chirality can effectively remove mirror symmetry. Besides, molecular chirality can ensure SC chirality to improve the probability of polar symmetry, which has been proposed by the ferroelectrochemistry concept.[45] Molecular chirality can be expected to provide a crucial connection for the ferroelectricity between the SC and LC phases. For the symmetry change during the phase transitions, the anisotropic group G_1 of the LC phase should be a subgroup of the isotropic liquid group G_0, and the configuration of G_1 depends on the molecular chirality. In turn, the symmetry of the SC phase should also be included in G_1, and a certain net spontaneous polarization could exist in the LC phase despite the loss of the long-range order due to the retention of the orientation order for molecular dipoles.[46−48]

In contrast to chiral smectic LCs, nematic or cholesteric LCs inherently possess higher fluidity and fewer defects, which is crucial to material durability and device performance in practical applications.[19,49−51] Nevertheless, whether ferroelectricity exists also in the cholesteric LCs with S_∞ symmetry is still unknown. In this work, we investigated a cholesteric liquid crystal, dihydrocholesteryl benzoate (BDC),[52] with a polar solid crystal phase of the $P2_1$ space group. However, unfortunately, no experimental evidence was detected to confirm its ferroelectricity in both SC and LC phases. The diversity and editability of organic molecules allow various chemical modifications to develop and optimize properties.[45,53−57] Notably, the H/F substitution strategy, which resembles H/D substitution isotopic substitution to some extent, has been developed as a novel and efficient chemical design strategy for the target design and performance optimization of molecular ferroelectric crystals.[45,54−57] However, it should be noted that the previous H/F substitution-designed molecular ferroelectric crystals only exhibit ferroelectricity in the SC phase and they show no LC phase.[45,54−57] Additionally, the parent compounds for previous H/F substitution were mainly based on the multi-component crystals with solid-to-solid phase transitions,[45,54−57] such as organic−inorganic (pyrrolidinium)MnCl₃ with a solid-to-solid phase transition at 295 K.[54] Since the incorporation of small-size F atoms enables the maintenance of the LC phase,

fluorination has also been applied to modify the properties of LCs like birefringence, stability, and melting point.[58−62]

Here, we employed the H/D and H/F substitution on the different positions of the phenyl group of the organic single-component parent molecule BDC with LC phase but without solid-to-solid phase transition (Scheme 1). Through the reasonable H/F substitution on the fourth position, we successfully designed a novel ferroelectric material dihydro-cholesteryl 4-fluorobenzoate (4-F-BDC) with switchable polarization existing in both SC and cholesteric LC phases. Compared to the parent BDC, the fluorinated 4-F-BDC adopts a lower symmetric polar $P1$ space group. More importantly, the introduction of fluorine in 4-F-BDC brings about a new solid-to-solid (S-to-S) phase transition at 327 K (T_{s-s}), distinct from the cases of H/D and H/F substitution on other positions of the phenyl group of BDC (Scheme 1) and rarely found in previously reported cases of H/F substitution,[54−57] which provides a variable for the polarization switching of 4-F-BDC. To our knowledge, 4-F-BDC is the first ferroelectric with novel dual-ferroelectricity in both SC and cholesteric LC phases. This pioneering work injects new vitality into the old ferroelectric field and sheds light on the further exploration of more excellent ferroelectrics with SC and cholesteric LC ferroelectric phases for potential applications in next-generation electro-optical devices.

RESULTS AND DISCUSSION

We synthesized the BDC, dihydrocholesteryl benzoate-4-d (4-d-BDC), dihydrocholesteryl benzoate-d_5 (d_5-BDC), dihydro-cholesteryl 2-fluorobenzoate (2-F-BDC), dihydrocholesteryl 3-fluorobenzoate (3-F-BDC), dihydrocholesteryl pentafluoro-benzoate (PF-BDC), and 4-F-BDC by the reaction of dihydrocholesterol and respective benzoic acid. Their crystals were easily prepared by the slow evaporation of the respective ethyl acetate solutions. Single-crystal X-ray diffraction determinations indicate that the SC phase of BDC crystallizes in the monoclinic system with a chiral and polar space group $P2_1$ (Table S1 and Figure S1). The differential scanning calorimetry (DSC) analysis reveals that BDC undergoes no S-to-S phase transition but a solid-to-liquid crystal (S-to-LC) phase transition at the transition temperature (T_{S-LC}) of 413 K (Figure 1a). The LC phase then transforms to a liquid phase (LP) at the clearing point of 430 K. The H/D substitution on the fourth position of the phenyl group of BDC maintains the crystal symmetry of the polar $P2_1$ space group and the phase
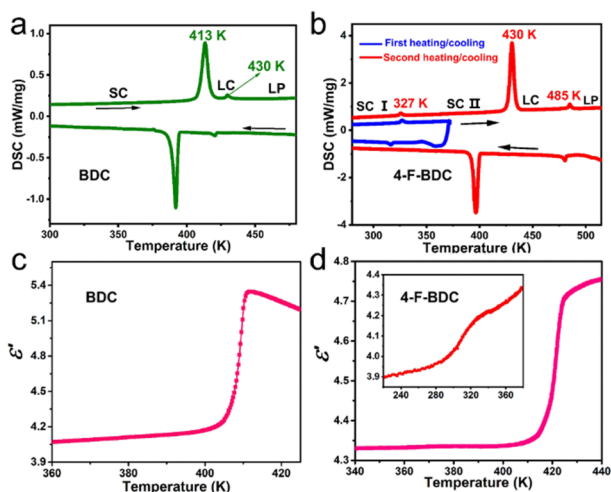
Figure 1. Phase transition properties. DSC curves of (a) BDC and (b) 4-F-BDC upon heating and cooling. Temperature-dependent real part (ε') of dielectric constant of (c) BDC and (d) 4-F-BDC.

transition behaviors without S-to-S phase transition in 4-d-BDC (Figure S2 and Table S1). Even replacing all the H atoms of the phenyl group of BDC with D atoms, the crystal symmetry of the polar $P2_1$ space group and similar phase transition behaviors still remain in d_5-BDC (Figure S3 and Table S1). Although the $P2_1$ space group meets the requirement of polar crystal symmetry for ferroelectrics, similar to the parent BDC, no substantial evidence was detected to confirm the ferroelectricity 4-d-BDC and d_5-BDC. We then employed the H/F substitution on BDC. The H/F substitution on the second and third positions of the phenyl group of BDC, respectively, changes the crystal symmetry in 2-F-BDC and 3-F-BDC. However, 2-F-BDC and 3-F-BDC adopt the nonpolar $P2_12_12_1$ and $P4_12_12$ space groups, respectively (Table S1), both of which cannot meet the requirement of polar crystal symmetry for ferroelectrics. In addition, the phase transitions of 2-F-BDC and 3-F-BDC are similar to those of parent BDC (Figures S4 and S5). We also employed the pentafluoride substitution on the phenyl group of BDC, while the obtained PF-BDC keeps the polar $P2_1$ space group and the similar phase transition behaviors to the parent BDC, which thus also shows

no detectable ferroelectricity (Figure S6 and Table S1). However, after the H/F substitution on the fourth position of the phenyl group of BDC, the crystal symmetry reduces to a lower symmetric polar $P1$ space group in 4-F-BDC (Table S1), and 4-F-BDC shows different phase transitions behaviors with a new S-to-S phase transition (see below).

The different crystal symmetries of 2-F-BDC, 3-F-BDC, PF-BDC, PF-BDC, and 4-F-BDC indicate that the H/F substitution on the benzene ring of the BDC molecule has a position effect on the crystal symmetry. The parent BDC is polar with space group $P2_1$. After all five hydrogen atoms in the benzene ring have been replaced by fluorine, the spatial group of PF-BDC has not changed. This is more consistent with the common understanding that perfluorinated substitution does not change the symmetry of the benzene ring. The H/F substitution on the fourth position of the benzene ring changes its symmetry to some extent, causing the crystal symmetry to become polar space group $P1$ in 4-F-BDC. However, H/F substitution on the second and third positions completely changed the symmetry of the benzene ring, so that there is no symmetric element in the benzene ring. The crystal symmetry then changes remarkably to nonpolar space groups in 2-F-BDC and 3-F-BDC. We also calculated the electrostatic potential of the molecules before and after H/F substitution. As shown in Figures S7–S11, only H/F substitution on the second and third positions significantly changed the surface electrostatic potential of the molecules, making the molecular arrangement more prone to a nonpolar fashion. It is worth noting that although BDC, PF-BDC, and 4-F-BDC all have polar crystal symmetry, only the 4-F-BDC shows an S-to-S phase transition, which makes the 4-F-BDC molecules easily prone to reorientation and provides a variable for polarization switching, beneficial for the generation of ferroelectricity in 4-F-BDC.

The DSC curves of 4-F-BDC show that it undergoes an S-to-LC phase transition at T_{S-LC} of 430 K and an LC to LP phase transition at the clearing point 485 K (Figure 1b), with an LC window of 55 K. The S-to-LC phase transitions of 4-F-BDC and BDC were also confirmed from the variable-temperature powder X-ray diffraction (PXRD) data, where PXRD patterns at a wide-angle diffraction area in the SC phase vanish in the LC phase (Figures S12 and S13). Compared to BDC, fluorination enables 4-F-BDC to exhibit a higher T_{S-LC},
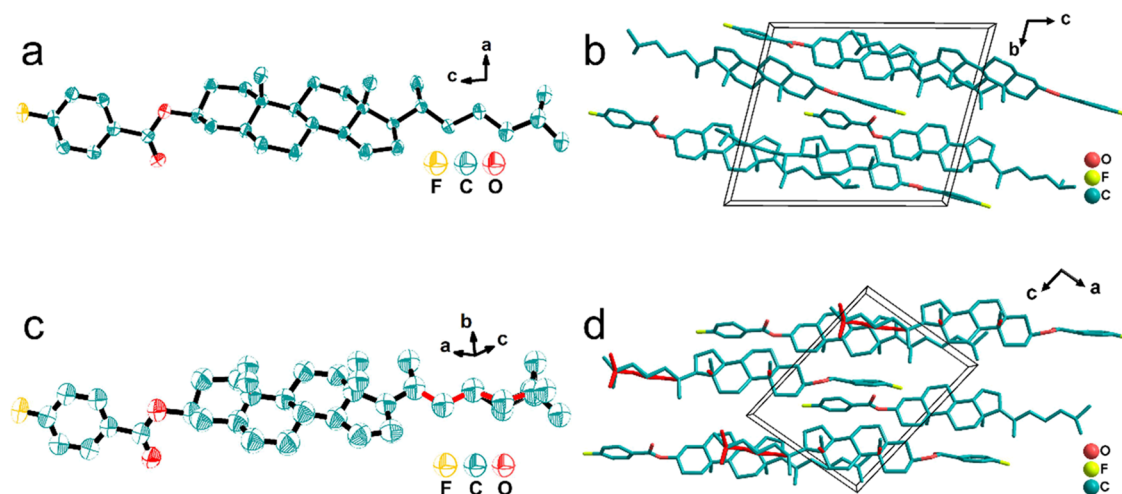

Figure 2. Crystal structures of 4-F-BDC. Thermal ellipsoid plots of the molecular unit in the SC I phase (a) and in the SC II phase (c), with ellipsoids drawn at the 30% probability level. Packing views of the unit cell in the SC I phase (b) and in the SC II phase (d).
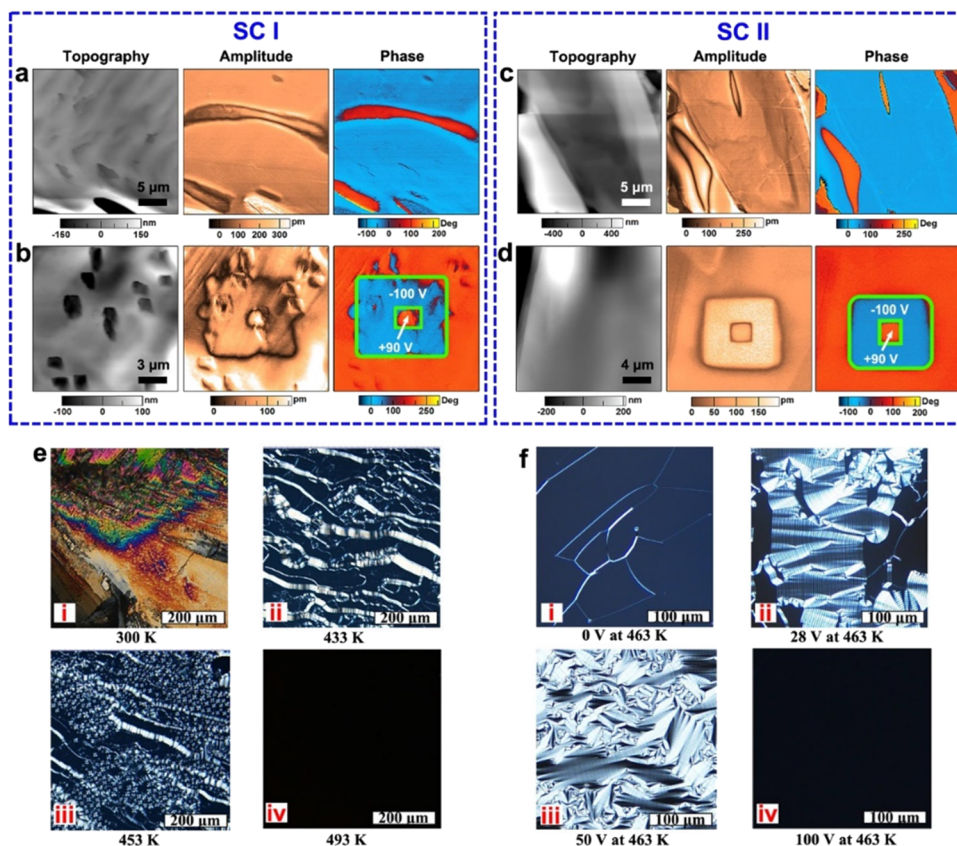
Figure 3. (a,b) Topography, vertical PFM amplitude, and phase images show the as-prepared domain structures (a) and reversible polarization switching characteristics (b) of the 4-F-BDC thin film in the phase I. (c,d) Topography, vertical PFM amplitude, and phase images show the domain structures (c) and reversible polarization switching characteristics (d) of the 4-F-BDC thin film in the phase II. (e) POM images for 4-F-BDC stimulated by thermal: the solid crystal phase (i), the cholesteric phase at different temperatures (ii-iii), and the isotropic phase (iv). (f) Optical texture of cholesteric phase (463 K) under different voltages.

higher clearing point, and broader LC phase. Note that the 4-F-BDC also experiences a new reversible S-to-S structural phase transition at about 327 K (T_{S-S}), which was rarely found in other cases of H/F substitution.[54−57] Correspondingly, the real part (ε') of dielectric constant of BDC and 4-F-BDC shows significant steplike anomalous changes near their respective T_{S-LC} (Figure 1c,d), while 4-F-BDC presents an additional dielectric anomaly at around T_{S-S}. Besides the phase transition behaviors, the second harmonic generation (SHG) measurements show that the strength of the SHG response in the SC phase is enhanced after fluorination (Figure S14). It is worth noting that in the second scan of DSC (Figure 1b), the peak of S-to-S phase transition is not observed in the cooling process, which is due to the fact that after cooling from above the clearing point, 4-F-BDC crystallizes into a new solid phase, and this new phase no longer exhibits phase transition behavior in the solid state (Figure S15).

We then get insight into the crystal structure of BDC and 4-F-BDC. The asymmetric unit of the SC crystal structure of BDC consists of three BDC molecules, which form a packing structure by the symmetrical operation of 2-fold screw axes along the *b*-axis (Figure S1). Fluorinated 4-F-BDC has two SC phases, both of which adopt the *P*1 space group of the lowest crystallographic symmetry. The asymmetric unit of its crystal structure in the SC I phase contains four 4-F-BDC molecules (Figure S16a), while that in the SC II phase halved to two molecules (Figure S16b). The 4-F-BDC molecules in SC I are ordered (Figure 2a,b) and become partially disordered in SC II

(Figure 2c,d). For a good structural refinement result, some carbon atoms, mainly from the chiral side alkyl, were split into two equivalent positions according to a certain occupancy rate to model a disorder state (Figure 2c). From the packing view, due to the same symmetry of the SC I and SC II phases, the two phases have a similar molecular packing, while the cell volume halves from the SC I to SC II phase. The PXRD data of 4-F-BDC also show the structural change from the SC I to SC II phase, as reflected from the merging of some PXRD diffraction peaks in SC II (Figure S17).

The polar crystal structures of BDC and 4-F-BDC illustrate their permanent dipole moment for spontaneous polarization. Thus, we calculated the dipole moment of single molecules of BDC and 4-F-BDC (Figures S18 and S19). The results show that the dipole moments of these two molecules increase sequentially with increasing atomic number (Table S2). The direction of the 4-F-BDC molecular dipole is parallel to the carbon−oxygen single bond (Figure S19), while the direction of the BDC molecular dipole is almost perpendicular to the direction of the long axis of the molecule (Figure S18). Furthermore, in order to estimate the ferroelectric polarization of the crystals, we employed the Berry phase method to gain the total value of ferroelectric polarization, from which the polarization with 78.2, 114.5, and 374.2 nC/cm^2 can be extracted for the crystals of BDC, 4-F-BDC in its SC I phase and SC II phase, respectively (Table S2). Due to the crystallographic symmetry requirement, the polarization of the BDC crystal is along the polar *b*-axis, while the polarization

along a- and c-axis is zero. In contrast, the polarization vectors of the 4-F-BDC crystal on the a-, b-, and c-axis are 84.2, 77.1, and 9.7 nC/cm^2, respectively. The difference in the polarization value mainly comes from different molecular dipole and their arrangement patterns in each crystal. It needs to be mentioned that no substantial evidence was detected to confirm the polarization switchability of the BDC crystal, which may not be ferroelectric. In contrast, fluorinated 4-F-BDC shows clear ferroelectricity with switchable polarization. This may be due to the fact that fluorination changes the crystal packing to make the molecules easily prone to reorientation, which can be foreshadowed by the appearance of solid−solid structural phase transitions of 4-F-BDC.

Typical pristine ferroelectric domains of thin films in two SC phases of 4-F-BDC are revealed by vertical PFM mappings of out-of-plane polarization, as shown in Figure 3a,c, which indicates the existence of spontaneous polarizations with different orientations in both solid phases. In order to intuitively demonstrate that the spontaneous polarization of the two solid phases can be switched by an external electric field, the samples are poled with a DC bias of −100 V and then +90 V to first switch the domains to the upward direction and then to the downward direction, respectively. Figure 3b,d shows the topography, vertical PFM amplitude, and phase images after the poling process. We obtained clear box-in-box bipolar states in both solid phases, and no morphology damage was observed. Therefore, the 4-F-BDC is ferroelectric in both SC I and SC II phases.

In addition to the domain switching measurement, we tested in situ the switching spectroscopy PFM (SS-PFM) of the two solid phases. As shown in Figure 4a,b, the phase loops and amplitude loops of the two solid phases show typical hysteresis and butterfly morphology, respectively, which fully proves that the spontaneous polarization of the two solid phases has ferroelectric switching behavior. PFM has been used for quantitatively measuring the local piezoresponse in ferro-

electric materials, wherein the sample is excited by an external actuator and its mechanical response at contact resonance with the cantilever is measured. By sweeping the excitation frequency across the contact resonance, the spectra of the cantilever response of the BDC and 4-F-BDC thin films can be obtained. As Figure 4c shows, the amplitude of the cantilever response for both thin films is fitted to a simple harmonic oscillator (SHO) model where the intrinsic amplitude, frequency, and quality factor (Q factor) are found for a certain excitation voltage. The amplitude signal has been corrected by dividing the Q factors, which represent the amplification factor of the signal. Such a process is repeated with several drive voltages ranging from 1 to 10 V and over 5 points on both thin films. From this, we obtained the relationship between the amplitude and the drive voltage of each film. The curves show a good linear relationship between the amplitude and the excitation voltage, and the slope represents the magnitude of the piezoelectric response. It can be seen from Figure 4d that the piezoelectric response of the 4-F-BDC thin film is 1.6 times that of the BDC thin film.

Polarizing optical microscopy (POM) is typically used to observe micro textures and identify the molecular orientations in various liquid crystal phases. At 300 K, the polycrystalline thin film sample of 4-F-BDC was sandwiched between two clean ITO glass substrates (Figure 3e(i)). Upon heating, the polycrystalline thin film was melted into a cholesteric phase near 430 K, accompanied by the appearance of distinct planar textures (Figure 3e(ii)). With further increase in temperature, the planar textures transform into small focal conic textures before the clearing point (485 K) and then enter an isotropic liquid state, which appears as a dark field under crossed polarizers (Figure 3e(iii) and (iv)). As shown in Figure S20, the BDC also exhibits cholesteric textures during the heating process, and the difference from 4-F-BDC is that the temperature range of the liquid crystal phase is very narrow.

Generally, when cholesteric liquid crystals are placed in a cell, the molecular orientations can be regulated by the applied electric field, thus showing various electro-optic effects. To reveal the electro-optic response of 4-F-BDC in the cholesteric phase, the behavior of its texture variation in a 4 μm anti-parallel liquid crystal cell under a DC electric field was investigated by POM. As the voltage increases, the planar textures (0 V) in the cholesteric phase transform into fingerprint textures (28 V), then focal conic textures (50 V), and finally homeotropic textures (100 V) with the helix completely untwisted (Figure 3f(i−iv)) and Figure 5a). Different from 4-F-BDC, the planar textures of BDC gradually disappeared under the stimulation of the DC electric field without an unwinding process (Figure S20).

As the direct evidences of ferroelectricity, the polarization−voltage ($P−V$) hysteresis loops were measured on 4-F-BDC samples to investigate the polarization switching behaviors in its SC and LC phases (Figure 5b−d). By using double-wave and triangular-wave methods, the typically well-shaped $P−V$ hysteresis loops of solid and liquid crystal phases were obtained, with the polarization values of about 93.7 (SC I phase), 350.3 (SC II phase), and 29.6 nC/cm^2 (LC phase). Such experimentally polarization values in SC phases match well with the theoretical calculated ones (Table S2). From the current−voltage curves measured in the LC phase, the 4-F-BDC exhibits two opposite current peaks in one cycle of the applied voltage, suggesting the reversible polarization switching process (Figure S21). The BDC shows two sharp triangular
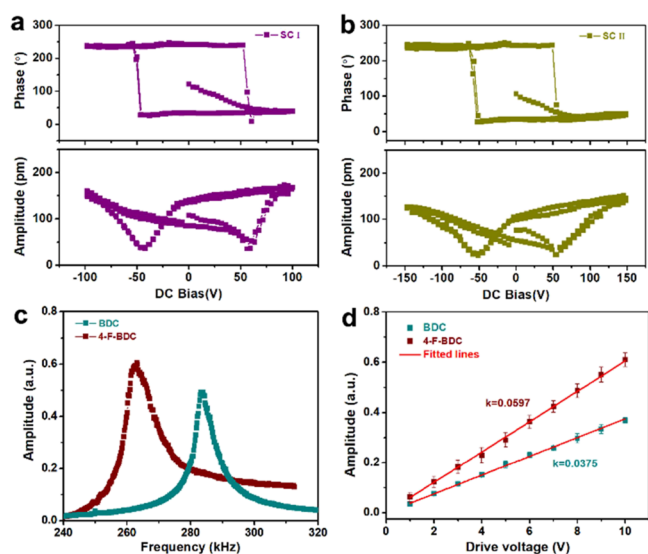

Figure 4. (a,b) Phase-voltage hysteresis loops and amplitude-voltage butterfly loops in both solid phases of 4-F-BDC obtained with SS-PFM. (c) Piezoresponse versus excitation frequency measured by vertical PFM on thin films of BDC and 4-F-BDC. (d) Q factor corrected amplitude signals as a function of AC drive voltages for the thin films of BDC and 4-F-BDC.
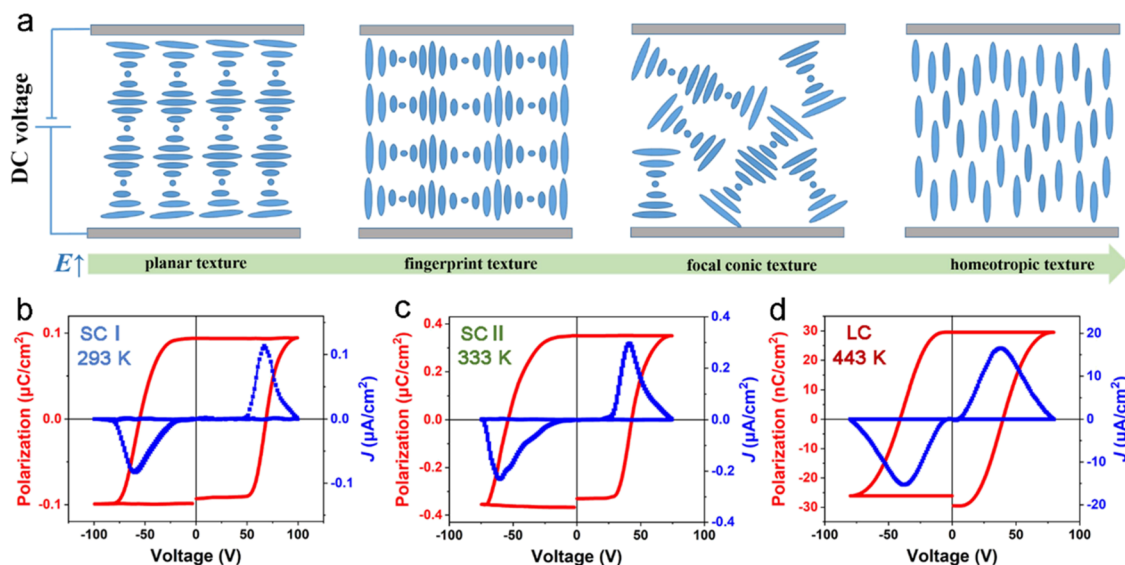
Figure 5. (a) Schematic diagram of various cholesteric textures of 4-F-BDC with increasing DC voltage in a 4 μm anti-parallel liquid crystal cell. Polarization-voltage hysteresis loops of 4-F-BDC in (b) SC I, (c) SC II, and (d) LC phase.

peaks with no hysteresis (Figure S21), revealing its non-ferroelectricity in the LC phase. The measured results indicate that 4-F-BDC is a ferroelectric material with switchable polarization in both its solid-crystal and liquid-crystal phases.

CONCLUSIONS

In summary, we reported a ferroelectric material dihydrocholesteryl 4-fluorobenzoate (4-F-BDC) with ferroelectricity in both SC and cholesteric LC phases, which was designed by using the reasonable H/F substitution on the fourth position of the phenyl group of parent dihydrocholesteryl benzoate (BDC). Compared to parent BDC with $P2_1$ symmetry, 4-F-BDC adopts a different stacking arrangement with the lowest symmetric polar $P1$ space group. Fluorination enables the 4-F-BDC to have a higher solid-to-liquid crystal phase transition temperature, a broader temperature window of the liquid crystal phase, a larger dipole moment for enhancing polarization, and a greater piezoelectric response. More importantly, the H/F substitution induces a new solid-to-solid phase transition in 4-F-BDC. The ferroelectric solid crystal and cholesteric liquid crystal phases of 4-F-BDC were identified and confirmed through rigorous experiments including polarization–voltage hysteresis loops. This work offers a viable case for the dual ferroelectricity in both solid and cholesteric liquid crystal phases of a single material and highlights the chemical strategy of H/F substitution in exploring novel ferroelectrics. Considering the abundant species and the structural modifiability of organic molecules, more excellent ferroelectrics with dual ferroelectricity in solid-crystal and liquid-crystal ferroelectric phases can be designed by chemical modification like H/F substitution.

EXPERIMENTAL SECTION

Materials

All reagents and solvents in the syntheses were of reagent grade and used without further purification. Dihydrocholesterol (1.94 g, 4.99 mmol), 4-fluorobenzoic acid (0.70 g, 5.00 mmol), 4-dimethylaminopyridine (2.20 g, 18.01 mmol), and dicyclohexylcarbodiimide (DCC, 3.09 g, 14.98 mmol) were added to a closed pressure-resistant bottle with 45 mL of dichloromethane (DCM), and the mixture was stirred

at 358 K for 48 h. Then, the resultant mixture was cooled, filtered, washed with DCM, and the solvent was removed under reduced pressure. The crude product was then purified by column chromatography (dichloromethane/petroleum ether = 1:5) to obtain a white solid of 4-F-BDC. The synthetic steps for BDC are similar to that of 4-F-BDC, except that 4-fluorobenzoic acid is replaced by benzoic acid. Similar synthetic processes can be referred to in the literature on the synthesis of fatty acid esters.[63,64] The colorless crystals of 4-F-BDC and BDC were easily prepared by the slow evaporation of their ethyl acetate solutions, respectively, at room temperature. As illustrated in Figures S22−S30, the purity of as-synthesized BDC and 4-F-BDC samples were demonstrated by the ^{1}H NMR (nuclear magnetic resonance), ^{13}C NMR, ^{19}F NMR, infrared spectra, UV−vis spectra, and PXRD patterns. The characteristic signal (δ −106.34, s) in the ^{19}F NMR spectrum confirmed the presence of the F−C bond in 4-F-BDC (Figure S26). The IR characteristic peaks of the C=O groups of BDC and 4-F-BDC are at around 1714 and 1716 cm^{-1}, respectively (Figure S27). For the 4-F-BDC, the IR characteristic peak of the C−F bond can be observed at 1230 cm^{-1}. Meanwhile, the UV−vis absorption spectra of BDC and 4-F-BDC display the clear absorption bands of the conjugated benzene ring (Figure S28). In addition, as shown in Figures S29 and S30, the experimental PXRD patterns of BDC and 4-F-BDC match well with the simulated ones from crystal structures. The detailed synthetic procedures of benzoic-4-d acid, 4-d-BDC, d_5-BDC, 2-F-BDC, 3-F-BDC, and PF-BDC are described in the Supporting Information, of which the purity was demonstrated by the NMR analyses (Figures S31−S45).

Thin-Film Preparation

The thin films of 4-F-BDC used for the PFM measurements and hysteresis loop testing are prepared through the drop-casting method. The precursor solution of 4-F-BDC was prepared by dissolving 10 mg of the crystals in 1 mL of tetrahydrofuran. Then, 40 mL of precursor solution was spread on a clean indium-doped tin oxide (ITO) glass substrate. The thin film was obtained after annealing at 373 K for 1 h.

Measurements

Methods for single-crystal and powder XRD, DSC, SHG, and dielectric measurements, P−V hysteresis loop test, PFM measurements, and related calculation conditions are described in the Supporting Information. Crystal structures have been deposited at the Cambridge Crystallographic Data Centre (deposition numbers CCDC: 2211583−2211585, 2234623−2234627) and can be obtained free of charge from the CCDC via www.ccdc.cam.ac.uk/getstructures.

ASSOCIATED CONTENT

Ⓢ Supporting Information

The Supporting Information is available free of charge at https://pubs.acs.org/doi/10.1021/jacsau.3c00059.

Synthesis of samples; measurement methods; NMR spectroscopy results; additional crystal structures; DSC curves; PXRD patterns; SHG curves; molecular configuration; POM images; current−voltage curves; NMR spectra; and crystal data (PDF)

AUTHOR INFORMATION

Corresponding Author

Wei-Qiang Liao − Ordered Matter Science Research Center, Nanchang University, Nanchang 330031, People's Republic of China; ⓞ orcid.org/0000-0002-5359-7037; Email: liaowq@ncu.edu.cn

Authors

Jun-Chao Liu − Ordered Matter Science Research Center, Nanchang University, Nanchang 330031, People's Republic of China

Hang Peng − Ordered Matter Science Research Center, Nanchang University, Nanchang 330031, People's Republic of China

Xiao-Gang Chen − Ordered Matter Science Research Center, Nanchang University, Nanchang 330031, People's Republic of China

Hui-Peng Lv − Ordered Matter Science Research Center, Nanchang University, Nanchang 330031, People's Republic of China

Xian-Jiang Song − Ordered Matter Science Research Center, Nanchang University, Nanchang 330031, People's Republic of China

Ren-Gen Xiong − Ordered Matter Science Research Center, Nanchang University, Nanchang 330031, People's Republic of China; ⓞ orcid.org/0000-0003-2364-0193

Complete contact information is available at:
https://pubs.acs.org/10.1021/jacsau.3c00059

Author Contributions

[†]J.-C.L. and H.P. contributed equally to this work. CRediT: **Xiao-Gang Chen** data curation, formal analysis, resources; **Hui-Peng Lv** data curation, formal analysis, resources; **Xian-Jiang Song** data curation, formal analysis, resources; **Ren-Gen Xiong** funding acquisition, project administration, supervision, writing-original draft, writing-review & editing; .

Author Contributions

CRediT: **Jun-Chao Liu** data curation, resources, writing-original draft; **Hang Peng** data curation, resources, writing-original draft; **Xiao-Gang Chen** data curation, formal analysis, resources; **Hui-Peng Lv** data curation, formal analysis, resources; **Xian-Jiang Song** data curation, formal analysis, resources; **Ren-Gen Xiong** funding acquisition, project administration, supervision, writing-original draft, writing-review & editing; **Wei-Qiang Liao** funding acquisition, project administration, supervision, writing-original draft, writing-review & editing.

Notes

The authors declare no competing financial interest.

REFERENCES

(1) Xu, Y. Ferroelectric materials and their applications; Elsevier, 2013.

(2) Beresnev, L. A.; Blinov, L. M.; Osipov, M. A.; Pikin, S. A. Ferroelectric Liquid Crystals. Mol. Cryst. Liq. Cryst. 1988, 158, 1−150.

(3) Hird, M. Ferroelectricity in liquid crystals—materials, properties and applications. Liq. Cryst. 2011, 38, 1467−1493.

(4) Valasek, J. Piezo-Electric and Allied Phenomena in Rochelle Salt. J. Phys. Rev. 1921, 17, 475−481.

(5) Liu, X.; Tan, P.; Ma, X.; Wang, D.; Jin, X.; Liu, Y.; Xu, B.; Qiao, L.; Qiu, C.; Wang, B.; Zhao, W.; Wei, C.; Song, K.; Guo, H.; Li, X.; Li, S.; Wei, X.; Chen, L.-Q.; Xu, Z.; Li, F.; Tian, H.; Zhang, S. Ferroelectric crystals with giant electro-opticproperty enabling ultracompact Q-switches. Science 2022, 376, 371−377.

(6) Haertling, G. H. Ferroelectric Ceramics: History and Technology. J. Am. Ceram. Soc. 1999, 82, 797−818.

(7) Horiuchi, S.; Tokunaga, Y.; Giovannetti, G.; Picozzi, S.; Itoh, H.; Shimano, R.; Kumai, R.; Tokura, Y. Above-room-temperature ferroelectricity in a single-component molecular crystal. Nature 2010, 463, 789.

(8) You, Y.-M.; Liao, W.-Q.; Zhao, D.; Ye, H.-Y.; Zhang, Y.; Zhou, Q.; Niu, X.; Wang, J.; Li, P.-F.; Fu, D.-W.; Wang, Z.; Gao, S.; Yang, K.; Liu, J.-M.; Li, J.; Yan, Y.; Xiong, R.-G. An organic-inorganic perovskite ferroelectric with large piezoelectric response. Science 2017, 357, 306−309.

(9) Anetai, H.; Takeda, T.; Hoshino, N.; Kobayashi, H.; Saito, N.; Shigeno, M.; Yamaguchi, M.; Akutagawa, T. Ferroelectric Alkylamide-Substituted Helicene Derivative with Two-Dimensional Hydrogen-Bonding Lamellar Phase. J. Am. Chem. Soc. 2019, 141, 2391−2397.

(10) Tang, Y.-Y.; Zeng, Y.-L.; Xiong, R.-G. Contactless Manipulation of Write−Read−Erase Data Storage in Diarylethene Ferroelectric Crystals. J. Am. Chem. Soc. 2022, 144, 8633−8640.

(11) Fang, Y.-H.; Liu, Z.; Zhou, S.; Fu, P.-X.; Wang, Y.-X.; Wang, Z.-Y.; Wang, Z.-M.; Gao, S.; Jiang, S.-D. Spin-Electric Coupling with Anisotropy-Induced Vanishment and Enhancement in Molecular Ferroelectrics. J. Am. Chem. Soc. 2022, 144, 8605−8612.

(12) Xiong, Y.-A.; Gu, Z.-X.; Song, X.-J.; Yao, J.; Pan, Q.; Feng, Z.-J.; Du, G.-W.; Ji, H.-R.; Sha, T.-T.; Xiong, R.-G.; You, Y.-M. Rational Design of Molecular Ferroelectrics with Negatively Charged Domain Walls. J. Am. Chem. Soc. 2022, 144, 13806−13814.

(13) Li, Q.; Wang, Q. Ferroelectric polymers and their energy related applications. Macromol. Chem. Phys. 2016, 217, 1228−1244.

(14) Chen, X.; Qin, H.; Qian, X.; Zhu, W.; Li, B.; Zhang, B.; Lu, W.; Li, R.; Zhang, S.; Zhu, L.; Santos, F. D. D.; Bernholc, J.; Zhang, Q. M. Relaxor ferroelectric polymer exhibits ultrahighelectromechanical coupling at low electric field. Science 2022, 375, 1418−1422.

(15) Scott, J. F. Applications of modern ferroelectrics. Science 2007, 315, 954.

(16) Martin, L. W.; Rappe, A. M. Thin-film ferroelectric materials and their applications. Nat. Rev. Mater. 2017, 2, 16087.

(17) Meyer, R. B.; Liebert, L.; Strzelecki, L.; Keller, P. Ferroelectric liquid crystals. J. Phys., Lett. 1975, 36, 69−71.

(18) Walba, D. Fast Ferroelectric Liquid-Crystal Electrooptics. Science 1995, 270, 250−250.

(19) Srivastava, A. K.; Chigrinov, V. G.; Kwok, H. S. Ferroelectric liquid crystals: Excellent tool for modern displays and photonics. J. Soc. Inf. Disp. 2015, 23, 253−272.

(20) Lagerwall, S. T.; Clark, N. A.; Dijon, J.; Clerc, J. F. Ferroelectric liquid crystals: The development of devices. Ferroelectrics 1989, 94, 3−62.

(21) Lagerwall, S. T. Ferroelectric and Antiferroelectric Liquid Crystals. Ferroelectrics 2004, 301, 15−45.

(22) Zhu, C.; Shao, R.; Reddy, R. A.; Chen, D.; Shen, Y.; Gong, T.; Glaser, M. A.; Korblova, E.; Rudquist, P.; Maclennan, J. E.; Walba, D. M.; Clark, N. A. Topological Ferroelectric Bistability in a Polarization-Modulated Orthogonal Smectic Liquid Crystal. *J. Am. Chem. Soc.* **2012**, *134*, 9681−9687.

(23) Filipic, C.; Levstik, A.; Levstik, I.; Blinc, R.; Zeks, B.; Glogarova, M.; Carlsson, T. Spontaneous polarization of helicoidal ferroelectric smectic C* liquid crystals. *Ferroelectrics* **1987**, *73*, 295−303.

(24) Sasaki, T.; Ikeda, T.; Ichimura, K. Photochemical Control of Properties of Ferroelectric Liquid Crystals: Photochemical Flip of Polarization. *J. Am. Chem. Soc.* **1994**, *116*, 625−628.

(25) Walba, D. M.; Dyer, D. J.; Sierra, T.; Cobben, P. L.; Shao, R. F.; Clark, N. A. Ferroelectric Liquid Crystals for Nonlinear Optics: Orientation of the Disperse Red 1 Chromophore along the Ferroelectric Liquid Crystal Polar Axis. *J. Am. Chem. Soc.* **1996**, *118*, 1211−1212.

(26) Vlahakis, J. Z.; Wand, M. D.; Lemieux, R. P. Photoinduced Polarization Inversion in a Ferroelectric Liquid Crystal Using an Ambidextrous Chiral Thioindigo Dopant. *J. Am. Chem. Soc.* **2003**, *125*, 6862−6863.

(27) Reddy, R. A.; Zhu, C.; Shao, R.; Korblova, E.; Gong, T.; Shen, Y.; Garcia, E.; Glaser, M. A.; Maclennan, J. E.; Walba, D. M.; Clark, N. A. Spontaneous Ferroelectric Order in a Bent-Core Smectic Liquid Crystal of Fluid Orthorhombic Layers. *Science* **2011**, *332*, 72−77.

(28) Ki Yoon, D.; Deb, R.; Chen, D.; Körblova, E.; Shao, R.; Ishikawa, K.; Rao, N. V. S.; Walba, D. M.; Smalyukh, I. I.; Clark, N. A. Organization of the polarization splay modulated smectic liquid crystal phase by topographic confinement. *Proc. Natl. Acad. Sci. U. S. A.* **2010**, *107*, 21311−21315.

(29) Walba, D. M.; Korblova, E.; Huang, C. C.; Shao, R. F.; Nakata, M.; Clark, N. A. Reflection Symmetry Breaking in Achiral Rod-Shaped Smectic Liquid Crystals? *J. Am. Chem. Soc.* **2006**, *128*, 5318−5319.

(30) Kishikawa, K.; Nakahara, S.; Nishikawa, Y.; Kohmoto, S.; Yamamoto, M. A Ferroelectrically Switchable Columnar Liquid Crystal Phase with Achiral Molecules: Superstructures and Properties of Liquid Crystalline Ureas. *J. Am. Chem. Soc.* **2005**, *127*, 2565−2571.

(31) McCubbin, J. A.; Tong, X.; Wang, R. Y.; Zhao, Y.; Snieckus, V.; Lemieux, R. P. Directed Metalation Route to Ferroelectric Liquid Crystals with a Chiral Fluorenol Core: The Effect of Restricted Rotation on Polar Order. *J. Am. Chem. Soc.* **2004**, *126*, 1161−1167.

(32) Maly, K. E.; Wand, M. D.; Lemieux, R. P. Bistable Ferroelectric Liquid Crystal Photoswitch Triggered by a Dithienylethene Dopant. *J. Am. Chem. Soc.* **2002**, *124*, 7898−7899.

(33) Lemieux, R. P. Chirality Transfer in Ferroelectric Liquid Crystals. *Acc. Chem. Res.* **2001**, *34*, 845−853.

(34) Chen, X.; Korblova, E.; Dong, D.; Wei, X.; Shao, R.; Radzihovsky, L.; Glaser, M. A.; Maclennan, J. E.; Bedrov, D.; Walba, D. M.; Clark, N. A. First-principles experimental demonstration of ferroelectricity in a thermotropic nematic liquid crystal: Polar domains and striking electro-optics. *Proc. Natl. Acad. Sci. U. S. A.* **2020**, *117*, 14021−14031.

(35) Lavrentovich, O. D. Ferroelectric nematic liquid crystal, a century in waiting. *Proc. Natl. Acad. Sci. U. S. A.* **2020**, *117*, 14629−14631.

(36) Zhao, X.; Zhou, J.; Li, J.; Kougo, J.; Wan, Z.; Huang, M.; Aya, S. Spontaneous helielectric nematic liquid crystals: Electric analog to helimagnets. *Proc. Natl. Acad. Sci. U. S. A.* **2021**, *118*, No. e2111101118.

(37) Sebastián, N.; Cmok, L.; Mandle, R. J.; de la Fuente, M. R.; Drevenšek Olenik, I.; Čopič, M.; Mertelj, A. Ferroelectric-Ferroelastic Phase Transition in a Nematic Liquid Crystal. *Phys. Rev. Lett.* **2020**, *124*, No. 037801.

(38) Feng, C.; Saha, R.; Korblova, E.; Walba, D.; Sprunt, S. N.; Jákli, A. Electrically Tunable Reflection Color of Chiral Ferroelectric Nematic Liquid Crystals. *Adv. Opt. Mater.* **2021**, *9*, No. 2101230.

(39) Barboza, R.; Marni, S.; Ciciulla, F.; Mir, F. A.; Nava, G.; Caimi, F.; Zaltron, A.; Clark, N. A.; Bellini, T.; Lucchetti, L. Explosive electrostatic instability of ferroelectric liquid droplets on ferroelectric solid surfaces. *Proc. Natl. Acad. Sci. U. S. A.* **2022**, *119*, No. e2207858119.

(40) Mandle, R. J.; Sebastián, N.; Martinez-Perdiguero, J.; Mertelj, A. On the molecular origins of the ferroelectric splay nematic phase. *Nat. Commun.* **2021**, *12*, 4962.

(41) Song, Y.; Li, J.; Xia, R.; Xu, H.; Zhang, X.; Lei, H.; Peng, W.; Dai, S.; Aya, S.; Huang, M. Development of emergent ferroelectric nematic liquid crystals with highly fluorinated and rigid mesogens. *Phys. Chem. Chem. Phys.* **2022**, *24*, 11536−11543.

(42) Li, J.; Xia, R.; Xu, H.; Yang, J.; Zhang, X.; Kougo, J.; Lei, H.; Dai, S.; Huang, H.; Zhang, G.; Cen, F.; Jiang, Y.; Aya, S.; Huang, M. How Far Can We Push the Rigid Oligomers/Polymers toward Ferroelectric Nematic Liquid Crystals? *J. Am. Chem. Soc.* **2021**, *143*, 17857−17861.

(43) Vertogen, G.; De Jeu, W. H. *Thermotropic liquid crystals, fundamentals*; Springer Series in Chemical Physics; Springer Science & Business Media, 2012; Vol *45*.

(44) Song, X.-J.; Chen, X.-G.; Liu, J.-C.; Liu, Q.; Zeng, Y.-P.; Tang, Y.-Y.; Li, P.-F.; Xiong, R.-G.; Liao, W.-Q. Biferroelectricity of a homochiral organic molecule in both solid crystal and liquid crystal phases. *Nat. Commun.* **2022**, *13*, 6150.

(45) Liu, H.-Y.; Zhang, H.-Y.; Chen, X.-G.; Xiong, R.-G. Molecular Design Principles for Ferroelectrics: Ferroelectrochemistry. *J. Am. Chem. Soc.* **2020**, *142*, 15205−15218.

(46) Grosso, G.; Parravicini, G. P. *Solid state physics*, Academic Press, 2013.

(47) Resta, R. Theory of the electric polarization in crystals. *Ferroelectrics* **1992**, *136*, 51−55.

(48) Vainshtein, B. K.; Fridkin, V. M.; Indenbom, V. L. *Modern crystallography II: Structure of crystals*; Springer, 1982; Vol. *21*.

(49) Nishikawa, H.; Shiroshita, K.; Higuchi, H.; Okumura, Y.; Haseba, Y.; Yamamoto, S.; Sago, K.; Kikuchi, H. A Fluid Liquid-Crystal Material with Highly Polar Order. *Adv. Mater.* **2017**, *29*, No. 1702354.

(50) Mitov, M. Cholesteric Liquid Crystals with a Broad Light Reflection Band. *Adv. Mater.* **2012**, *24*, 6260−6276.

(51) Li, J.; Nishikawa, H.; Kougo, J.; Zhou, J.; Dai, S.; Tang, W.; Zhao, X.; Hisai, Y.; Huang, M.; Aya, S. Development of ferroelectric nematic fluids with giant-ε dielectricity and nonlinear optical properties. *Sci. Adv.* **2021**, *7*, No. eabf5047.

(52) Carr, S. G.; Khoo, S. K.; Luckhurst, G. R.; Smith, H. The Orientational Order in Cholesteric Liquid Crystals. *J. Mol. Cryst. Liq. Cryst.* **1978**, *45*, 161−181.

(53) Bie, J.; Yang, D.-B.; Ju, M.-G.; Qiang, J.; Pan, Q.; You, Y.-M.; Fa, W.; Zeng, X.-C.; Chen, S. Molecular Design of Three-Dimensional Metal-Free A(NH$_4$)X$_3$ Perovskites for Photovoltaic Applications. *JACS Au* **2021**, *1*, 475−483.

(54) Ai, Y.; Chen, X. G.; Shi, P. P.; Tang, Y. Y.; Li, P. F.; Liao, W. Q.; Xiong, R. G. Fluorine Substitution Induced High T_c of Enantiomeric Perovskite Ferroelectrics: (R)- and (S)-3-(Fluoropyrrolidinium)MnCl$_3$. *J. Am. Chem. Soc.* **2019**, *141*, 4474−4479.

(55) Zhang, H.-Y.; Zhang, Z.-X.; Song, X.-J.; Chen, X.-G.; Xiong, R.-G. Two-Dimensional Hybrid Perovskite Ferroelectric Induced by Perfluorinated Substitution. *J. Am. Chem. Soc.* **2020**, *142*, 20208−20215.

(56) Tang, Y. Y.; Xie, Y.; Ai, Y.; Liao, W. Q.; Li, P. F.; Nakamura, T.; Xiong, R.-G. Organic Ferroelectric Vortex−Antivortex Domain Structure. *J. Am. Chem. Soc.* **2020**, *142*, 21932−21937.

(57) Xie, Y.; Ai, Y.; Zeng, Y.-L.; He, W.-H.; Huang, X.-Q.; Fu, D.-W.; Gao, J.-X.; Chen, X.-G.; Tang, Y.-Y. The Soft Molecular Polycrystalline Ferroelectric Realized by Fluorination Effect. *J. Am. Chem. Soc.* **2020**, *142*, 12486−12492.

(58) Hird, M. Fluorinated liquid crystals—properties and applications. *Chem. Soc. Rev.* **2007**, *36*, 2070−2095.

(59) Goswami, D.; Debnath, A.; Mandal, P. K.; Weglowska, D.; Dabrowski, R.; Czuprynski, K. Effect of chain length and fluorination on the dielectric and electro-optic properties of three partially

fluorinated biphenylyl benzoate rigid core based ferroelectric liquid crystals. *Liq. Cryst.* **2016**, *43*, 1548−1559.

(60) Haldar, S.; Dey, K. C.; Sinha, D.; Mandal, P. K.; Haase, W.; Kula, P. X-ray diffraction and dielectric spectroscopy studies on a partially fluorinated ferroelectric liquid crystal from the family of terphenyl esters. *Liq. Cryst.* **2012**, *39*, 1196−1203.

(61) Kitazume, T.; Ohnogi, T.; Ito, K. Design and synthesis of new fluorinated ferroelectric liquid-crystalline polymers. *J. Am. Chem. Soc.* **1990**, *112*, 6608−6615.

(62) Walba, D. M.; Razavi, H. A.; Clark, N. A.; Parmar, D. S. Design and synthesis of new ferroelectric liquid crystals. 5. Properties of some chiral fluorinated FLCs: a direct connection between macroscopic properties and absolute configuration in a fluid phase. *J. Am. Chem. Soc.* **1988**, *110*, 8686−8691.

(63) Boden, E. P.; Keck, G. E. Proton-transfer steps in Steglich esterification: a very practical new method for macrolactonization. *J. Org. Chem.* **1985**, *50*, 2394−2395.

(64) Farshori, N. N.; Banday, M. R.; Zahoor, Z.; Rauf, A. DCC/DMAP mediated esterification of hydroxy and non-hydroxy olefinic fatty acids with β-sitosterol: In vitro antimicrobial activity. *Chin. Chem. Lett.* **2010**, *21*, 646−650.